ELSEVIER

Physica A 253 (1998) 541–554

PHYSICA A

High-frequency photoabsorption by an ion immersed in a plasma as calculated from Bloch's hydrodynamic model

K. Ishikawa, B.U. Felderhof*

Institut für Theoretische Physik A, R.W.T.H. Aachen, Templergraben 55, 52056 Aachen, Germany

Received 28 December 1997

Abstract

The high-frequency behavior of the photoabsorption cross section of an ion immersed in a plasma is investigated in the framework of the Thomas–Fermi model, supplemented with Bloch's hydrodynamic equations. It is shown that the singular nature of the electron density profile near the point nucleus, derived in Thomas–Fermi approximation, causes enhanced high-frequency absorption proportional to the inverse square of frequency. According to an exact quantummechanical relation the electron density profile is not singular. It is shown that in the hydrodynamic model a regular density profile leads to a photoabsorption cross section which decays as the inverse sixth power of frequency. Thus for a regular density profile collective effects described in the hydrodynamic model rapidly become less important at high frequency. In this regime the photoabsorption cross section is dominated by single electron inverse bremsstrahlung.

PACS: 52.25.Mq; 71.45.Gm; 31.15.Bs; 78.20.ci
Keywords: Photoabsorption; Plasma; Dielectric function

1. Introduction

In previous work [1–3] we have studied photoabsorption in dense plasmas on the basis of Bloch's hydrodynamic model [4]. Quantummechanical transitions were left out of consideration, so that the theory certainly cannot do justice to the rich absorption spectra seen in experiment. On the other hand, the treatment accounts for the collective motion arising from the interaction of the electron cloud of a selected ion with the surrounding plasma. Plasma effects are omitted in theories which take a single atom or ion as their starting point [5–7]. It is expected that the approximate

* Corresponding author. Tel.: +49 241 807019; Fax: +49 241 8888188; e-mail: ufelder@physik.rwth-aachen.de.

PII S0378-4371(98)00065-X

hydrodynamic treatment provides a qualitative picture of the effect of the surrounding plasma on the photoabsorption spectrum for frequencies of the order of the plasma frequency.

We have studied, in particular, the photoabsorption cross section of an ion immersed in a plasma described in Thomas–Fermi approximation [3]. A surprising feature of the calculation was that at high frequency, the cross section decays with only the inverse square of frequency, with a coefficient independent of temperature and pressure. The behavior is identical to that found by Ball et al. [8] for an atom in vacuum at zero temperature. This would suggest that at high frequency collective effects dominate the cross section. In comparison, the cross section for single electron inverse bremsstrahlung decays with the inverse cube of frequency [9]. Although one may take the view that at high frequency the hydrodynamic equations do not apply anyway [8], the result is somewhat disturbing and in our opinion demands fuller investigation.

We show in the following that the enhanced high-frequency absorption is due to the singularity in the electron density profile arising in the Thomas–Fermi model for an ion with a point nucleus. The enhanced absorption disappears if the electron density profile is regular. The Thomas–Fermi model can be modified in such a way that the electron density profile satisfies an exact quantummechanical rule [10]. For the density profile thus made regular the hydrodynamic theory leads to a decay of the cross section with the inverse sixth power of frequency. Consequently, at high frequency the total cross section is dominated by single electron inverse bremsstrahlung.

The calculation of the high-frequency behavior of the cross section within the hydrodynamic model is nontrivial and has an interest of its own. The electron charge density at a particular frequency satisfies a diffusion-type equation. Thus, the calculation is related to studies of short-time effects in Brownian motion theory [11–13].

2. Photoabsorption

We consider photoabsorption by an ion of charge Ze centered at the origin and immersed in a plasma. In thermal equilibrium the electron density, averaged over the positions of the remaining ions, is radially symmetric. We denote the mean electron density profile by $\bar{n}_0(r)$. In Bloch's hydrodynamic model [1,4] one also needs the profile $\bar{\vartheta}_0(r)$ corresponding to the average of the local derivative $(\partial\mu/\partial n)_{\bar{n}_0}$ of the electron chemical potential with respect to density. At large distance from the selected ion the density $\bar{n}_0(r)$ tends to the uniform value $n_0^{(0)}$, and the profile $\bar{\vartheta}_0(r)$ tends to the corresponding value $\vartheta_0^{(0)}$, given by the equilibrium equation of state. In order to calculate the photoabsorption cross section in the framework of Bloch's hydrodynamic model one considers linear response of the system to a uniform oscillating electric field $\boldsymbol{E}^{(0)}(t) = \boldsymbol{E}_\omega^{(0)} \exp(-i\omega t)$. The hydrodynamic equations for the electron gas are

linearized to [1]

$$\frac{\partial n_1}{\partial t} + \nabla \cdot (\bar{n}_0 \boldsymbol{v}_1) = 0\,,$$

$$m\frac{\partial \boldsymbol{v}_1}{\partial t} = -\nabla(\bar{\vartheta}_0 n_1) + e\nabla\phi_1\,, \tag{2.1}$$

where $n_1(\boldsymbol{r},t)$ is the deviation of the electron density from the equilibrium profile, $\boldsymbol{v}_1(\boldsymbol{r},t)$ is the flow velocity, m is the electron mass, $-e$ the electron charge, and $\phi_1(\boldsymbol{r},t)$ is the deviation of the electrostatic potential from its equilibrium value. The potential ϕ_1 is related to the density n_1 by Poisson's equation $\nabla^2\phi_1 = 4\pi e n_1$. Putting

$$n_1(\boldsymbol{r},t) = n_\omega(\boldsymbol{r})\exp(-i\omega t), \quad \rho_\omega = -en_\omega\,, \tag{2.2}$$

one finds for the electron charge density $\rho_\omega(\boldsymbol{r})$

$$\nabla \cdot [\bar{n}_0 \nabla(\bar{\vartheta}_0 \rho_\omega)] + e^2 \nabla \cdot \left(\bar{n}_0 \nabla \int \frac{\rho_\omega(\boldsymbol{r}')}{|\boldsymbol{r}-\boldsymbol{r}'|} d\boldsymbol{r}'\right) + m\omega^2\rho_\omega = e^2 \boldsymbol{E}_\omega^{(0)} \cdot \nabla \bar{n}_0\,. \tag{2.3}$$

We write this equation in the form

$$\nabla \cdot D \cdot [\nabla\rho_\omega + (\nabla U)\rho_\omega] + \omega^2\rho_\omega - \frac{e^2}{m}\nabla \cdot (\bar{n}_0 \boldsymbol{E}_\omega) = \frac{e^2}{m}\boldsymbol{E}_\omega^{(0)} \cdot \nabla \bar{n}_0 \tag{2.4}$$

with diffusion coefficient D and potential U defined by

$$D = \frac{1}{m}\bar{n}_0\bar{\vartheta}_0, \qquad U = \ln[\bar{\vartheta}_0/\vartheta_0^{(0)}]\,, \tag{2.5}$$

and with electric field $\boldsymbol{E}_\omega$ given by $\boldsymbol{E}_\omega = -\nabla\phi_\omega$. The induced electric dipole moment $\boldsymbol{p}_\omega^{(1)}$ is defined by

$$\boldsymbol{p}_\omega^{(1)} = \int \boldsymbol{r}\rho_\omega(\boldsymbol{r})\, d\boldsymbol{r}\,. \tag{2.6}$$

The frequency-dependent photoabsorption cross section can be calculated from the polarizability $\alpha_1'(\omega)$ defined by [1]

$$\boldsymbol{p}_\omega^{(1)} = \alpha_1'(\omega)\boldsymbol{E}_\omega^{(0)}\,. \tag{2.7}$$

In the present study we are interested, in particular, in the behavior of the photoabsorption cross section at high frequency. It will be shown in the following that this is dominated by the short distance behavior of the mean profiles $\bar{n}_0(r)$ and $\bar{\vartheta}_0(r)$. We assume that the profiles have power-law behavior of the form

$$\bar{n}_0(r) \sim r^{-\alpha}, \quad \bar{\vartheta}_0(r) \sim r^{\beta} \quad \text{as } r \to 0\,. \tag{2.8}$$

For the Thomas–Fermi model with a point nucleus and the Fermi–Dirac ideal gas equation of state the exponents are $\alpha = \frac{3}{2}$ and $\beta = \frac{1}{2}$ at any temperature [3]. We refer to this model as the TFPI model. More generally, we consider a class of models with a range of freely variable parameters α and β. For the regular density profile the exponents are $\alpha = \beta = 0$.

3. Dimensionless equations

For mathematical purposes it is convenient to transform the basic equation (2.4) to a dimensionless form. Thus, we introduce the dimensionless distance x by

$$r = Z^{-1/3} b\, a_0\, x, \qquad b = \frac{1}{2}\left(\frac{3\pi}{4}\right)^{2/3}, \tag{3.1}$$

where $a_0 = \hbar^2/me^2$ is the Bohr radius. Correspondingly, we define the dimensionless profiles $\hat{n}_0(x)$ and $\hat{\vartheta}_0(x)$ by

$$\overline{n}_0(r) = \frac{Z^2}{b^3 a_0^3}\hat{n}_0(x), \qquad \overline{\vartheta}_0(r) = Z^{-2/3} e^2 b^2 a_0^2 \hat{\vartheta}_0(x). \tag{3.2}$$

The dimensionless frequency and electric field are defined by

$$\Omega = \frac{\hbar a_0}{Ze^2}\omega, \qquad \hat{\boldsymbol{E}} = \frac{b^2 a_0^2}{Z^{5/3} e}\boldsymbol{E}_\omega. \tag{3.3}$$

From Eq. (2.5) we define the dimensionless diffusion coefficient $\hat{D}(x)$ by

$$\hat{D} = \hat{n}_0 \hat{\vartheta}_0. \tag{3.4}$$

Moreover, we define the dimensionless charge density $\hat{\rho}(x)$ by

$$\rho_\omega(\boldsymbol{r}) = \frac{Z^2 e}{b^3 a_0^3}\hat{\rho}(\boldsymbol{x}). \tag{3.5}$$

Then Eq. (2.4) takes the dimensionless form

$$\frac{\partial}{\partial \boldsymbol{x}} \cdot \hat{D} \cdot \left[\frac{\partial \hat{\rho}}{\partial \boldsymbol{x}} + \left(\frac{\partial U}{\partial \boldsymbol{x}}\right)\hat{\rho}\right] - p\hat{\rho} - \frac{\partial}{\partial \boldsymbol{x}} \cdot (\hat{n}_0 \hat{\boldsymbol{E}}) = \hat{\boldsymbol{E}}^{(0)} \cdot \frac{\partial \hat{n}_0}{\partial \boldsymbol{x}}, \tag{3.6}$$

where $p = -b^3\Omega^2$. The field $\hat{\boldsymbol{E}}(\boldsymbol{x})$ is given by the solution of the electrostatic equation

$$\frac{\partial}{\partial \boldsymbol{x}} \cdot \hat{\boldsymbol{E}} = 4\pi\hat{\rho}. \tag{3.7}$$

In the TFPI model the profiles $\hat{n}_0(x)$ and $\hat{\vartheta}_0(x)$ are independent of the charge number Z.

We choose the z-axis in the direction of $\boldsymbol{E}_\omega^{(0)}$ and use spherical coordinates (r, θ, φ). By angular symmetry the charge density $\hat{\rho}(\boldsymbol{x})$ takes the form

$$\hat{\rho}(\boldsymbol{x}) = f(x)\cos\theta \tag{3.8}$$

with $f(x)$ satisfying the radial equation

$$\frac{d^2 f}{dx^2} + P\frac{df}{dx} + Qf - \frac{p}{\hat{D}}f + K_{\mathrm{op}} f = \frac{\hat{E}^{(0)}}{\hat{D}}\frac{d\hat{n}_0}{dx} \tag{3.9}$$

with coefficient functions $P(x)$ and $Q(x)$ given by

$$P(x)=\frac{2}{x}+\frac{\hat{D}'}{\hat{D}}+U',$$

$$Q(x)=-\frac{2}{x^2}+\left(\frac{2}{x}+\frac{\hat{D}'}{\hat{D}}\right)U'+U''-\frac{4\pi}{\hat{\vartheta}_0}. \tag{3.10}$$

The prime indicates differentiation with respect to x. The linear operator K_{op} is defined by

$$K_{\mathrm{op}}f=\frac{4\pi}{3}\frac{\hat{n}_0{}'}{\hat{D}}\left[\int_x^\infty f(x')\,dx'-\frac{2}{x^3}\int_0^x x'^3 f(x')\,dx'\right]. \tag{3.11}$$

The second term in Eq. (3.9) can be eliminated by means of the transformation

$$f(x)=g(x)\exp(H(x)), \tag{3.12}$$

with

$$H(x)=-\frac{1}{2}\int_{x_0}^x P(x')\,dx', \tag{3.13}$$

where x_0 is a fixed value. This leads to the integro-differential equation

$$\frac{d^2g}{dx^2}+\left[Q-\frac{1}{4}P^2-\frac{1}{2}P'\right]g-\frac{p}{\hat{D}}g+e^{-H}K_{\mathrm{op}}e^{H}g=\hat{E}^{(0)}\frac{e^{-H}}{\hat{D}}\hat{n}_0{}'. \tag{3.14}$$

We introduce the new variable

$$\xi=\int_0^x\frac{1}{\sqrt{\hat{D}(x')}}\,dx' \tag{3.15}$$

and the function

$$h(\xi)=\frac{1}{[\hat{D}(x)]^{1/4}}g(x). \tag{3.16}$$

Then $h(\xi)$ satisfies the integro-differential equation

$$\frac{d^2h}{d\xi^2}-ph-Wh+M_{\mathrm{op}}h=\hat{E}^{(0)}e^{-H}\hat{D}^{-1/4}\hat{n}_0' \tag{3.17}$$

with function $W(\xi)$ given by

$$W=\hat{D}\left[\frac{1}{4}P^2+\frac{1}{2}P'-Q-\frac{1}{4}\frac{\hat{D}''}{\hat{D}}+\frac{3}{16}\frac{\hat{D}'^2}{\hat{D}^2}\right] \tag{3.18}$$

and linear operator M_{op} defined by

$$M_{\mathrm{op}}=\hat{D}^{3/4}e^{-H}K_{\mathrm{op}}e^{H}\hat{D}^{1/4}. \tag{3.19}$$

The primes in Eq. (3.18) again indicate differentiation with respect to x. From Eq. (2.8) we find

$$\hat{D} \approx D_0 x^{\beta-\alpha} \quad \text{as } x \to 0 \tag{3.20}$$

with a coefficient D_0. From Eq. (3.10) for $\beta < 2$

$$P \approx \frac{2-\alpha+2\beta}{x}, \qquad Q \approx \frac{-2+\beta(1-\alpha+\beta)}{x^2} \qquad \text{as } x \to 0\,. \tag{3.21}$$

Hence, the function $W(\xi)$ can be expressed as

$$W(\xi) = \frac{\lambda}{\xi^2} + V(\xi)\,, \tag{3.22}$$

where the first term dominates for small ξ and $V(\xi)$ is the remainder. The coefficient λ is found to be

$$\lambda = \frac{32 - 12\alpha + 4\beta + 3\alpha^2 + 2\alpha\beta - \beta^2}{4(2+\alpha-\beta)^2}\,. \tag{3.23}$$

Finally, we define the function $\psi(\xi)$ by

$$h(\xi) = \hat{E}^{(0)} \sqrt{\xi}\, \psi(\xi)\,. \tag{3.24}$$

Then Eq. (3.17) transforms to

$$\frac{d^2\psi}{d\xi^2} + \frac{1}{\xi}\frac{d\psi}{d\xi} - p\psi - \left(\frac{\nu^2}{\xi^2} + \mathscr{V}_{\mathrm{op}}\right)\psi = R_0\,, \tag{3.25}$$

with coefficient

$$\nu^2 = \lambda + \frac{1}{4} = \frac{9 - 2\alpha + \alpha^2}{(2+\alpha-\beta)^2}\,, \tag{3.26}$$

linear operator

$$\mathscr{V}_{\mathrm{op}} = V + \frac{1}{\sqrt{\xi}} M_{\mathrm{op}} \sqrt{\xi}\,, \tag{3.27}$$

and on the right-hand side the function

$$R_0(\xi) = \frac{1}{\sqrt{\xi}} e^{-H} \hat{D}^{-1/4} \hat{n}_0'\,. \tag{3.28}$$

We assume that the effect of the operator $\mathscr{V}_{\mathrm{op}}$ is sufficiently weak that Eq. (3.25) can be solved by iteration. Thus, we consider the zero-order solution ψ_0 as the solution of the equation

$$\frac{d^2\psi_0}{d\xi^2} + \frac{1}{\xi}\frac{d\psi_0}{d\xi} - p\psi_0 - \frac{\nu^2}{\xi^2}\psi_0 = R_0\,. \tag{3.29}$$

This is an inhomogeneous Bessel equation of order ν which can be solved explicitly.

In Green's function form

$$\psi_0 = G_{\mathrm{op}} R_0 \,. \tag{3.30}$$

The complete solution of Eq. (3.25) can be expressed as the Born series

$$\psi = \sum_{j=0}^{\infty} \psi_j \tag{3.31}$$

with

$$\psi_j = G_{\mathrm{op}} \mathscr{V}_{\mathrm{op}} \psi_{j-1}, \quad j = 1, 2, \ldots \,. \tag{3.32}$$

In analogy to Eq. (3.30) we write the complete solution as

$$\psi = G_{\mathrm{op}} R \,. \tag{3.33}$$

In the next section, we show that at high frequency, i.e. at large p, only the first term ψ_0 matters.

4. High-frequency behavior

The polarizability $\alpha_1'(\omega)$ can be expressed as an integral of the solution $\psi(\xi, p)$ of Eq. (3.25). The high-frequency behavior of the polarizability follows from the behavior of the solution $\psi(\xi, p)$ for large p. From Eqs. (2.6), (3.5), and (3.8) we find

$$p_\omega^{(1)} = \frac{4\pi}{3} Z^{2/3} e b a_0 \int_0^\infty x^3 f(x, p)\, dx \,. \tag{4.1}$$

Hence, the polarizability is given by

$$\alpha_1'(\omega) = \frac{4\pi}{3} \frac{b^3 a_0^3}{Z} \int_0^\infty \xi w(\xi) \psi(\xi, p)\, d\xi \tag{4.2}$$

with weight function

$$w(\xi) = \frac{1}{\sqrt{\xi}} x^3 \hat{D}^{3/4} e^H \,. \tag{4.3}$$

We denote the integral in Eq. (4.2) by

$$A(p) = \int_0^\infty \xi w(\xi) \psi(\xi, p)\, d\xi \,. \tag{4.4}$$

It is useful to transform the integral into an integral over wavenumbers. To that purpose we consider the Hankel transforms [14]

$$w_\nu(k) = \int_0^\infty \xi J_\nu(k\xi) w(\xi)\, d\xi\,,$$

$$\psi_\nu(k, p) = \int_0^\infty \xi J_\nu(k\xi) \psi(\xi, p)\, d\xi\,. \tag{4.5}$$

The inverse transforms are

$$w(\xi) = \int_0^\infty k J_\nu(k\xi) w_\nu(k)\, dk\,,$$

$$\psi(\xi, p) = \int_0^\infty k J_\nu(k\xi) \psi_\nu(k, p)\, dk\,. \tag{4.6}$$

By substitution into Eq. (4.4) we find the Parseval formula

$$A(p) = \int_0^\infty k w_\nu(k) \psi_\nu(k, p)\, dk\,. \tag{4.7}$$

Next, we consider the explicit form of the Green's function corresponding to the linear operator G_{op} appearing in Eq. (3.29). The solution of Eq. (3.29) is given by

$$\psi_0(\xi, p) = \int_0^\infty G(\xi, \xi', p) R_0(\xi')\, d\xi' \tag{4.8}$$

with Green's function

$$\begin{aligned} G(\xi, \xi', p) &= -I_\nu(q\xi) K_\nu(q\xi') \xi' \quad \text{for } \xi' > \xi\,, \\ &= -K_\nu(q\xi) I_\nu(q\xi') \xi' \quad \text{for } \xi' < \xi\,, \end{aligned} \tag{4.9}$$

where $I_\nu(z)$ and $K_\nu(z)$ are modified Bessel functions [15] and $q = \sqrt{p}$. For large positive p the Green's function has appreciable weight only for small distance $|\xi - \xi'|$. The Hankel transform of the Green's function with respect to its first argument is

$$G_\nu(k, \xi', p) = \frac{-1}{p + k^2} \xi' J_\nu(k\xi')\,, \tag{4.10}$$

as can be shown with the aid of Bessel function identities [16]. Hence, the Hankel transform $\psi_\nu(k, p)$ is given by

$$\psi_\nu(k, p) = \frac{-1}{p + k^2} R_\nu(k, p)\,. \tag{4.11}$$

Substituting this into Eq. (4.7) we find a spectral representation of the dimensionless polarizability $A(p)$. The behavior of the spectral density for large p is determined by the wavenumber dependence of the transforms $w_\nu(k)$ and $R_\nu(k,p)$ for large k. This in turn is determined by the behavior of the functions $w_\nu(\xi)$ and $R_\nu(\xi,p)$ for small ξ. From Eq. (2.8) and the transformations in the preceding section we find

$$w(\xi)\approx B\xi^\gamma, \quad R_0(\xi)\approx C\xi^\delta \quad \text{as } \xi\to 0\,, \tag{4.12}$$

with exponents

$$\gamma=\frac{3-\alpha}{2+\alpha-\beta}, \qquad \delta=\gamma-2\,. \tag{4.13}$$

For the TFPI model $\gamma=\frac{1}{2}$ and $\delta=-\frac{3}{2}$. It follows from Eqs. (3.30)–(3.33) and Eq. (4.10) that for large p the singular behavior of $R(\xi,p)$ is the same as that of $R_0(\xi)$. We find the behavior of the Hankel transforms $w_\nu(k)$ and $R_{0\nu}(k)$ for large k from the Weber–Schafheitlin formula [17]

$$\int_0^\infty \frac{J_\nu(t)}{t^{\nu-\mu+1}}\,dt=\frac{\Gamma(\frac{1}{2}\mu)}{2^{\nu-\mu+1}\Gamma(\nu-\frac{1}{2}\mu+1)}\,. \tag{4.14}$$

Hence, we obtain

$$w_\nu(k)\approx B\frac{2^{\gamma+1}\Gamma(\frac{\nu+\gamma}{2}+1)}{\Gamma(\frac{\nu-\gamma}{2})}k^{-\gamma-2} \quad \text{as } k\to\infty\,, \tag{4.15}$$

and for the transform $R_{0\nu}(k)$

$$R_{0\nu}(k)\approx C\frac{2^{\delta+1}\Gamma(\frac{\nu+\delta}{2}+1)}{\Gamma(\frac{\nu-\delta}{2})}k^{-\delta-2} \quad \text{as } k\to\infty\,. \tag{4.16}$$

For certain values of α and β the conditions of validity of Eq. (4.14) are violated, but an exponential convergence factor may be introduced, as shown by Watson [17], so that the asymptotic formulae (4.15) and (4.16) remain valid. Substituting into Eq. (4.7) and using Eq. (4.11) we find for the imaginary part of $A(p)$ on the negative p axis

$$\lim_{\varepsilon\to 0+}\operatorname{Im}A(p=-k^2+i\varepsilon)=-\frac{\pi}{2}w_\nu(k)R_\nu(k,-k^2+i0)\,. \tag{4.17}$$

We write the asymptotic form of the density profile as

$$\hat{n}_0(x)\approx N_0x^{-\alpha} \quad \text{as } x\to 0\,, \tag{4.18}$$

with a coefficient N_0. From Eqs. (4.15) and (4.16) we find for large k

$$-\frac{\pi}{2}w_\nu(k)R_{0\nu}(k)\approx \pi N_0\,D_0^{\frac{\gamma+\delta}{2}+1}\alpha(2+\alpha-\beta)^{\gamma+\delta+1} \times\frac{\Gamma(\frac{\nu+\gamma}{2}+1)\Gamma(\frac{\nu+\delta}{2}+1)}{\Gamma(\frac{\nu-\gamma}{2})\Gamma(\frac{\nu-\delta}{2})}k^{-\gamma-\delta-4}\,. \tag{4.19}$$

The coefficient D_0 was defined in Eq. (3.20). The extinction cross section as a function of frequency is given by [1]

$$\sigma_{\mathrm{ext}}(\omega) = \frac{\pi}{c}\sqrt{\omega^2 - \omega_{p0}^2}\,\mathrm{Im}\,\alpha_1'(\omega)\,, \tag{4.20}$$

where $\omega_{p0}^2 = 4\pi n_0^{(0)} e^2/m$ is the plasma frequency. The dimensionless cross section $\hat{\sigma}_{\mathrm{ext}}(\Omega)$ is defined by

$$\sigma_{\mathrm{ext}}(\omega) = \frac{4\pi e^2}{\hbar c} b^3 a_0^2 \hat{\sigma}_{\mathrm{ext}}(\Omega)\,, \tag{4.21}$$

and given by

$$\hat{\sigma}_{\mathrm{ext}}(\Omega) = \frac{4\pi}{3}\sqrt{\Omega^2 - \Omega_{p0}^2}\,\mathrm{Im}\,A(-b^3\Omega^2)\,. \tag{4.22}$$

From Eqs. (4.17) and (4.19) we find for the high-frequency behavior

$$\hat{\sigma}_{\mathrm{ext}}(\Omega) \approx S\Omega^{-\kappa} \quad \text{as } \Omega \to \infty \tag{4.23}$$

with exponent

$$\kappa = 3 + \gamma + \delta = \frac{8 - \alpha - \beta}{2 + \alpha - \beta} \tag{4.24}$$

and coefficient

$$S = \frac{4\pi^2}{3} N_0 D_0^{[(\gamma+\delta)/2]+1} \alpha (2 + \alpha - \beta)^{\gamma+\delta+1} \frac{\Gamma(\frac{\nu+\gamma}{2} + 1)\Gamma(\frac{\nu+\delta}{2} + 1)}{\Gamma(\frac{\nu-\gamma}{2})\Gamma(\frac{\nu-\delta}{2})} b^{-(3/2)(\gamma+\delta+4)}\,. \tag{4.25}$$

For the TFPI model $N_0 = 1/4\pi$, $D_0 = \frac{2}{3}$, $\alpha = \frac{3}{2}$, $\beta = \frac{1}{2}$, $\gamma = \frac{1}{2}$, $\delta = -\frac{3}{2}$. For that model the cross-section decays as Ω^{-2} and the coefficient becomes

$$S = \frac{512}{81\pi^2\sqrt{3}} \left[\frac{\Gamma(\frac{2\nu+1}{4})}{\Gamma(\frac{2\nu+3}{4})}\right]^2 = 0.70144 \quad \text{(TFPI)} \tag{4.26}$$

with $\nu = \sqrt{33}/6$. This agrees with the result of Ball et al. [8] for this model at zero temperature and with vanishing asymptotic electron density $n_0^{(0)}$. Our calculation shows that for the TFPI model the coefficient is independent of temperature and density $n_0^{(0)}$. The result is confirmed by numerical calculation, as shown in Fig. 1. For other models the exponent κ and the coefficient S depend on the exponents α and β defined in Eq. (2.8), and on the coefficients N_0 and D_0 defined in Eqs. (3.20) and (4.18).

5. Regular profile

The coefficient S in Eq. (4.25) vanishes for $\alpha = 0$. This indicates that for a regular density profile the calculation of the preceding section does not apply. In this section we consider the required modification.

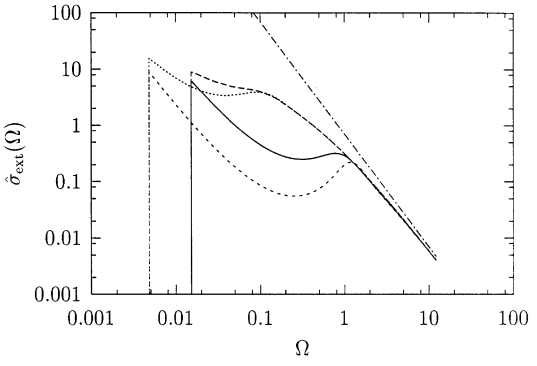

Fig. 1. The dimensionless cross section $\hat{\sigma}_{\rm ext}(\Omega)$ as a function of frequency Ω for the TFPI model at density $\hat{n}_0^{(0)} = 1.28 \times 10^{-5}$ and temperatures $\hat{T} = 0.0845$ (solid curve) and $\hat{T} = 0.00845$ (long dashes), and at density $\hat{n}_0^{(0)} = 1.28 \times 10^{-6}$ and temperatures $\hat{T} = 0.0845$ (short dashes) and $\hat{T} = 0.00845$ (dotted curve). At high frequencies all four curves tend to the asymptote $0.70144/\Omega^2$ as given by Eq. (4.26) (dash-dotted line).

Actually, the singular density profile is a peculiarity of the Thomas–Fermi model resulting from the incomplete treatment of quantummechanical effects. According to quantummechanics the exact electron density $n_0(r)$ and its derivative dn_0/dr are finite at the point nucleus and related by

$$\left.\frac{dn_0}{dr}\right|_{r=0} = -\frac{2Z}{a_0} n_0(0) \tag{5.1}$$

at any temperature [10]. We can modify the Thomas–Fermi model in such a way that Eq. (5.1) is satisfied by replacing the point nucleus by a diffuse spherical charge distribution [18]. Such a change will predominantly affect the high-frequency behavior of the photoabsorption cross section. By this procedure the singular density profile is changed into a regular one. We remark that the corrections for strongly bound electrons introduced by Scott [19] and Schwinger [20] give an electron density profile that still diverges at the origin. In a more detailed correction by Englert [21] the electron density is finite at the origin, but its derivative diverges there.

For a regular density profile both exponents α and β in Eq. (2.8) vanish, so that from Eq. (3.26) the order of the Bessel functions is $\nu = \frac{3}{2}$. From Eq. (4.13) the values of the exponents γ and δ are $\gamma = \frac{3}{2}$, $\delta = -\frac{1}{2}$. This shows that the denominator in Eq. (4.15) diverges, so that we must calculate the next term in the asymptotic expansion of $w_\nu(k)$ for large k.

We assume that the profiles $\hat{n}_0(x)$ and $\hat{\vartheta}_0(x)$ have the regular expansions

$$\begin{aligned} \hat{n}_0(x) &= N_0 + N_1 x + O(x^2)\,, \\ \hat{\vartheta}_0(x) &= T_0 + T_1 x + O(x^2)\,, \end{aligned} \tag{5.2}$$

where N_0 and N_1 are related by Eq. (5.1), and T_0 and T_1 are related to N_0 and N_1 by the equilibrium equation of state. From Eq. (3.4) we find

$$\hat{D}(x) = D_0 + D_1 x + O(x^2) \tag{5.3}$$

with

$$D_0 = N_0 T_0, \quad D_1 = N_0 T_1 + N_1 T_0 . \tag{5.4}$$

We define coefficients H_0, H_1 from the function $H(x)$ in Eq. (3.13) as

$$\exp(H(x)) = \frac{H_0}{x}[1 + H_1 x] + O(x^2) . \tag{5.5}$$

The derivative of the potential $U(x)$ is

$$U'(x) = \frac{T_1}{T_0} + O(x) . \tag{5.6}$$

We therefore find from Eqs. (3.10) and (3.13)

$$H_1 = -\frac{N_1}{2N_0} - \frac{T_1}{T_0} . \tag{5.7}$$

From Eq. (4.3) we find that the weight function $w(\xi)$ has the expansion

$$w(\xi) = B\xi^{3/2} + B_1 \xi^{5/2} + O(\xi^{7/2}) \tag{5.8}$$

with coefficients

$$B = D_0^{7/4} H_0, \qquad B_1 = B\left[\frac{5D_1}{4\sqrt{D_0}} + H_1\sqrt{D_0}\right] . \tag{5.9}$$

The function $R_0(\xi)$ defined in Eq. (3.28), has the expansion

$$R_0(\xi) = C\sqrt{\xi} + O(\xi^{3/2}) , \tag{5.10}$$

with coefficient

$$C = \frac{D_0^{1/4} N_1}{H_0} . \tag{5.11}$$

For the high-frequency behavior of the cross section we find finally

$$\hat{\sigma}_{\mathrm{ext}}(\Omega) \approx S_1 \Omega^{-6} \quad \text{as } \Omega \to \infty \tag{5.12}$$

with coefficient

$$S_1 = \frac{2^{61/2}}{3^8 \pi^6} B_1 C \approx 240.7 B_1 C . \tag{5.13}$$

In the product $B_1 C$ the coefficient H_0 cancels. We find

$$B_1 C = \tfrac{1}{4} N_1 D_0^{3/2} [N_0 T_1 + 3N_1 T_0] . \tag{5.14}$$

We have performed an explicit calculation for the Thomas–Fermi model in order to estimate the frequency range in which the asymptotic result (5.12) becomes dominant.

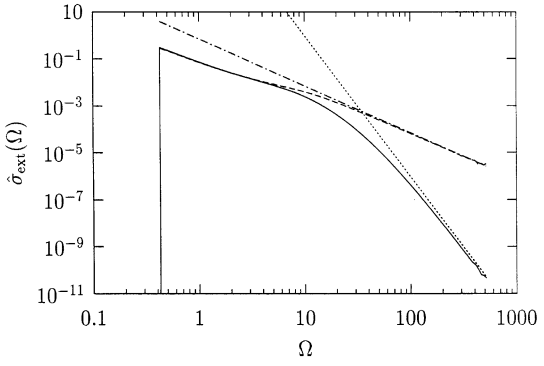

Fig. 2. The dimensionless cross section $\hat{\sigma}_{\rm ext}(\Omega)$ as a function of Ω for the Thomas–Fermi model at reduced temperature $\hat{T}=1$, asymptotic electron density $\hat{n}_0^{(0)}=10^{-2}$, and nuclear charge number $Z=13$ (solid curve). The density profile has been made regular at the origin by the device discussed in Section 5. At high frequencies the cross section tends to the asymptote $S_1\Omega^{-6}$ with $S_1=971689$, as given by Eq. (5.13) (dotted line). We compare with the cross section for the TFPI model with the same parameters (long dashes). This tends to the asymptote $S\Omega^{-2}$ with $S=0.70144$ (dash-dotted line).

We make the electron density profile regular by replacing the Coulomb potential of the point nucleus by the potential produced by the spherical charge density

$$\rho_n(r)=Ze\frac{k^2}{\pi}\frac{e^{-2kr}}{r} \tag{5.15}$$

with a coefficient k chosen such that the relation (5.1) is satisfied. In contrast to the TFPI model the resulting density profile no longer scales with the charge number Z. The charge density (5.15) differs from the one in Ref. [18], but has the advantage that it is positive everywhere. In Fig. 2 we plot the dimensionless cross section $\hat{\sigma}_{\rm ext}(\Omega)$ as a function of Ω for the Thomas–Fermi model at reduced temperature $\hat{T}=1$ and asymptotic electron density $\hat{n}_0^{(0)}=10^{-2}$ for the above nuclear charge density with $Z=13$. At high frequency, the cross section is dominated by the asymptotic result (5.12). We compare with the cross section as calculated for the TFPI model with the same parameters. In the intermediate frequency regime the cross section for the two models is the same.

6. Conclusion

A calculation of the photoabsorption cross section of an ion immersed in a plasma within the framework of the Thomas–Fermi model supplemented with Bloch's hydrodynamic equations showed surprisingly strong absorption at high frequencies [3]. The preceding analysis shows that the enhanced absorption is due to the singular electron density profile near the point nucleus. The singularity is a peculiar feature of the Thomas–Fermi approximation. In reality, the density profile is regular near the nucleus. A calculation of the cross section on the basis of Bloch's hydrodynamic model

shows that for a regular profile the cross section decays with the inverse sixth power of frequency at high frequency. The coefficient of the power law depends on the electron density at the nucleus and on the equilibrium equation of state of the electron gas. The rapid decay with frequency indicates that at high frequency collective absorption becomes less important. At high frequency, the photoabsorption cross section is dominated by single electron inverse bremsstrahlung.

Acknowledgements

We thank Dr. T. Blenski for stimulating discussion. This work was supported by the Project SILASI, TMR Network Contract, No. ERB FMRX-CT96-0043.

References

[1] B.U. Felderhof, T. Blenski, B. Cichocki, Physica A 217 (1995) 175.
[2] B.U. Felderhof, T. Blenski, B. Cichocki, Physica A 217 (1995) 196.
[3] K. Ishikawa, B.U. Felderhof, T. Blenski, B. Cichocki, submitted for publication.
[4] F. Bloch, Z. Phys. 81 (1933) 363.
[5] A. Zangwill, P. Soven, Phys. Rev. A 21 (1980) 1561.
[6] F. Grimaldi, A. Grimaldi-Lecourt, M.W.C. Dharma-wardana, Phys. Rev. A 32 (1985) 1063.
[7] F. Perrot, M.W.C. Dharma-wardana, Phys. Rev. Lett. 71 (1993) 797.
[8] J.A. Ball, J.A. Wheeler, E.L. Firemen, Rev. Mod. Phys. 45 (1973) 333.
[9] B.H. Armstrong, R.W. Nicholls, Emission, Absorption and Transfer of Radiation in Heated Atmospheres, Pergamon, Oxford, 1972, p. 202.
[10] C.C.J. Roothaan, A.W. Weiss, Rev. Mod. Phys. 32 (1960) 194.
[11] M. Kac, Am. Math. Monthly 73 (1966) 1.
[12] P.G. de Gennes, C.R. Acad. Sci. Paris 295 (1982) 1061.
[13] P.P. Mitra, P.N. Sen, L.M. Schwartz, Phys. Rev. B 47 (1993) 8565.
[14] H.S. Carslaw, J.C. Jaeger, Conduction of Heat in Solids, Clarendon, Oxford, 1973, p. 458.
[15] M. Abramowitz, I.A. Stegun, Handbook of Mathematical Functions, Dover, New York, 1965.
[16] E.T. Whittaker, G.N. Watson, A Course of Modern Analysis, Cambridge University Press, Cambridge, 1958, p. 381.
[17] G.N. Watson, A Treatise on the Theory of Bessel Functions, Cambridge University Press, Cambridge, 1966, p. 391.
[18] R.G. Parr, S.K. Ghosh, Proc. Natl. Acad. Sci. USA 83 (1986) 3577.
[19] J. Scott, Philos. Mag. 43 (1952) 859.
[20] J. Schwinger, Phys. Rev. A 22 (1980) 1827.
[21] B.-G. Englert, Semiclassical Theory of Atoms, Springer, Berlin, 1988.